We are IntechOpen, the world's leading publisher of Open Access books
Built by scientists, for scientists

6,900
Open access books available

185,000
International authors and editors

200M
Downloads

154
Countries delivered to

Our authors are among the

TOP 1%
most cited scientists

12.2%
Contributors from top 500 universities

CLARIVATE ANALYTICS
BOOK CITATION INDEX
INDEXED

WEB OF SCIENCE™

Selection of our books indexed in the Book Citation Index
in Web of Science™ Core Collection (BKCI)

Interested in publishing with us?
Contact book.department@intechopen.com

Numbers displayed above are based on latest data collected.
For more information visit www.intechopen.com

4

Semiconductor Optical Amplifiers and their Application for All Optical Wavelength Conversion

Oded Raz
Eindhoven University of Technology
The Netherlands

1. Introduction

All optical networks and switches are envisioned as a solution to the increasing complexity and power consumption of today's communication networks who rely on optical fibers for the transmission of information but use electronics at the connecting points on the network (nodes) to perform the switching operation. All optical networks, in contrast, will use simple signalling methods to trigger all optical switches to forward the optical data, from one optical fiber to another, without the need to convert the information carried by the optical signal into an electric one. This may save up to 50% of the total power consumption of the switches and will allow for simple scaling of the transmission rates. While all optical networks may offer significant breakthroughs in power consumption and network design, they fall back on one essential aspect, contention resolution. In traditional communication networks and in particular those who carry data (which has long surpassed voice traffic, in bandwidth), the nodes on the network use huge amounts of electronic random access memory (RAM) to store incoming data while waiting for their forwarding to be carried out. The storage of data, also called buffering, is essential in resolving contention which occurs when two incoming streams of data need to be forwarded to the same output port at the same time. In contrast all optical switches, who do not convert the data signals into the electrical domain, cannot use electronic buffers for contention resolution. They can however use the unique properties of light signals which at moderate power levels can propagate along the same transmission media without interference if they have different wavelengths. This means that if two competing light signals need to be switched to the same output port, their successful forwarding can be accomplished by assigning them different wavelength. This can be done completely in the optical domain by means of all optical wavelength conversion.

Large optical networks, require optical amplifiers for signal regeneration, especially so if the signal is not regenerated through optical to electrical to optical conversion. Semiconductor Optical Amplifiers (SOAs) are a simple, small size and low power solution for optical amplification. However, unlike fiber based amplifiers such as EDFAs, they suffer from a larger noise figure, which severely limits their use for long haul optical communication networks. Nevertheless, SOAs have found a broad area of applications in non-linear all optical processing, as they exhibit ultra fast dynamic response and strong non-linearities,

which are essential for the implementation of all optical networks and switches. This means that for a most essential function such as all optical wavelength conversions, SOAs are an excellent solution.

Wavelength conversion based on SOAs has followed several trajectories which will be detailed in the following sections. In section 2 we discuss how data patterns can be copied from one optical carrier to another based on the modulation of gain and phase experienced by an idle optical signal in the presence of a modulated carrier. Section 3 is devoted for the use of Kerr effect based wavelength conversion, and specifically to wavelength conversion based on degenerate four wave mixing (FWM). In section 4 we discuss how the introduction of new types of SOAs based on quantum dot gain material (QDSOA) has lead to advances in all optical wavelength conversion due to their unique properties. We conclude the chapter in section 5 where we point at future research directions and the required advancement in SOA designs which will allow for their large scale adoption in all optical switches.

2. Cross gain and cross phase modulation based convertors

When biased above their transparency current, SOAs may deliver considerable optical gain with a typical operational bandwidth of several tens of nanometers. However, since the gain mechanism is based on injection of carriers, the introduction of modulated optical carriers, and especially of short high peak power pulses such as those used for Opitcal Time Domain Multiplexing systems (OTDM), result in severe modulation of gain bearing majority carriers leading to undesirable cross talk in case multiple channels are introduced into the SOA (Inoue, 1989). The gain of an SOA recovers on three different timescales. Ultrafast gain recovery, driven by carrier–carrier scattering takes place at sub-picoseconds timescale (Mark & Mork, 1992). Furthermore, carrier–phonon interactions contribute to the recovery of the amplifier on a timescale of a few picoseconds (Mark & Mork, 1992). Finally, on a tens of picoseconds to nanosecond timescale, there is a contribution driven by electron–hole interactions. This last recovery mechanism dominates the eventual SOA recovery. Careful design of the active layer in the amplifier, injection efficiency and carrier confinement plays a role in the final recovery time which can vary between several hundreds of picoseconds to as low as 25 pico seconds for specially designed Quantum Well structures (CIP white paper , 2008). During the recovery of gain and carriers from the introduction of an optical pulse, the refractive index of the SOA wave guiding layer is also altered, so that not only the gain but also the phase of the CW signals travelling through the device is modulated. These two phenomena, termed Cross Gain Modulation (XGM) and Cross Phase Modulation (XPM), severely limit the use of SOAs for amplification of optical signals in Wavelength Division Multiplexed (WDM) networks.

Yet, the coupling of amplitude modulation of one optical channel into the amplitude and phase of other optical carriers travelling in the same SOAs has caught the attention of researchers working on all optical networks as a simple manner of duplicating data from one wavelength to another, a process also known as wavelength conversion.

Early attempts to exploit XGM in SOAs were already reported in 1993 (Wiesenfeld et al, 1993) where conversion of Non Return to Zero (NRZ) data signal was achieved at a bit rate of 10Gb/s and a tuning range of 17nm. These were later followed with demonstrations of conversion at increasingly higher bit rates but due to the low peak to average power ratio of NRZ signals (which dominated optical communications until the end of the 1990's) could not exceed 40Gb/s (and even this was only made possible with the use of two SOAs nested in a Mach Zehnder interferometer (Miyazaki et al, 2007).

ODTM systems which are based on short optical pulses interleaved together to achieve an effective data rate in the hundreds of Gb/s was conceived as an alternative to WDM for multiplexing data channels into the optical domain. The large peak to average power ratio associated with this transmission technique means that the carrier depletion effect is much stronger leading to a more pronounced drop in gain. For OTDM signals many methods have been proposed to allow high bit-rate All Optical Wavelength Conversion (AOWC) based on an SOA. Higher bit-rate operation was achieved by employing a fiber Bragg grating (FBG) (Yu et al, 1999), or a waveguide filter (Dong et al, 2000). In (Miyazaki et al, 2007), a switch using a differential Mach–Zehnder interferometer with SOAs in both arms has been introduced. The latter configuration allows the creation of a short switching window (several picoseconds), although the SOA in each arm exhibits a slow recovery. A delayed interferometric wavelength converter, in which only one SOA has been implemented, is presented in (Nakamura et al, 2001). The operation speed of this wavelength converter can reach 160 Gb/s and potentially even 320Gb/s (Liu et al, 2005) and allows also photonic integration (Leuthold et al, 2000). This concept has been analyzed theoretically in (Y. Ueno et al, 2002). The delayed interferometer also acts as an optical filter. Nielsen and Mørk (Nielsen & Mørk, 2004) present a theoretical study that reveals how optical filtering can increase the modulation bandwidth of SOA-based switches. Two separate approaches for filter assisted conversion can be considered, inverted and non-inverted.

Inverted wavelength conversion

In case an inversion stage is added after optical filtering, it is possible to obtain ultra high speed conversion (bit rate >300 Gb/s) by combining XGM and XPM. This can be most easily understood by looking at Fig. 1. The CW optical signal (or CW probe) is filtered by a Guassian shaped filter which is detuned relative to the probe's wavelength (peak of filter is placed at a shorter wavelength - blue shifted).
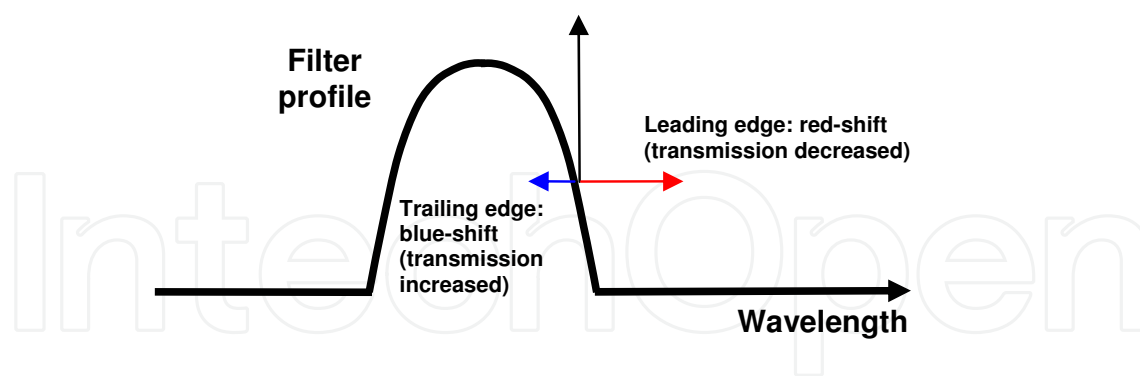

Fig. 1. Operation principle of detuned filtering conversion

As the pump light hits the SOA (leading edge of the pulse), carrier depletion results in a drop of gain as well as a phase change which leads to a wavelength shift to a longer wavelength (red-shift). This means that for the CW probe, on top of the drop in gain, a further drop in power is observed as the signal is further pushed out of the filter's band pass. Once the pump signal has left the SOA, carrier recovery begins, with a steady increase in gain and carrier concentration. The latter is responsible for a blue-shift in the probe's wavelength, which implies that the CW probe is now pushed into the middle of the filter's band, further increasing the output power, and effectively speeding up the eventual

recovery of the probe signal. As a result, the net intensity at the filter output is constant although the actual carrier recovery may continue far after the pump pulse has passed the SOA (see Fig. 2).
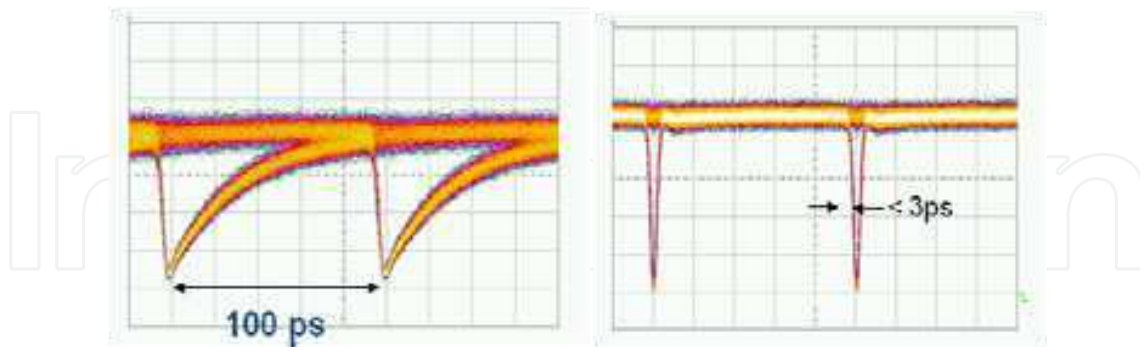

Fig. 2. Effect of filter detuning on probe recovery; (Left) no detuning, (Right) optimum detuning

Using this method, AOWC has been demonstrated at speeds up to and including 320 Gb/s (Y. Liu et al, 2005). The main limitation in extending the technique to even higher bit-rates is that as bit-rate increases the peak to mean power ratio drops, so that patterning effects dominate the performance of the converter and the obtained eye opening of the converted signal degrades. Further limitations of this conversion technique arise from the need to include after the SOA and optical filter, an inversion stage, which essentially suppresses the original CW optical carrier leading to poor optical signal to noise ratio at the output of the complete converter. Typical reported conversion penalties are dependent on the bit rate and might be as high as 10dB for 320Gb/s conversion.

Non-inverted wavelength conversion

For the non inverted conversion, although both XGM and XPM occur with the introduction of a short high power pulse into the SOA, it is mostly the effect of phase modulation that is utilized. As discussed above, during the introduction of a short optical pump pulse into the SOA, the changing levels of carriers leads to changes in refractive index which modulate the phase and frequency of the CW probe. By using a very sharp flat top filter (see Fig. 3), the induced frequency shifts can be converted to amplitude variations, thus having direct rather than inverted relation to the pump signal. Since both red and blue shifting of the probe's wavelength occurs, it is in principal possible to place the sharp filter so that the pass band is
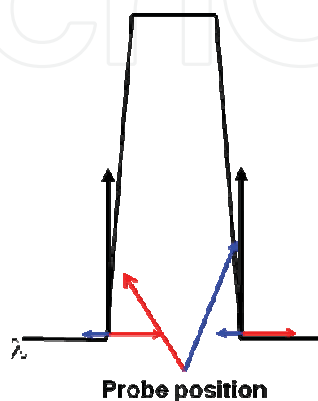

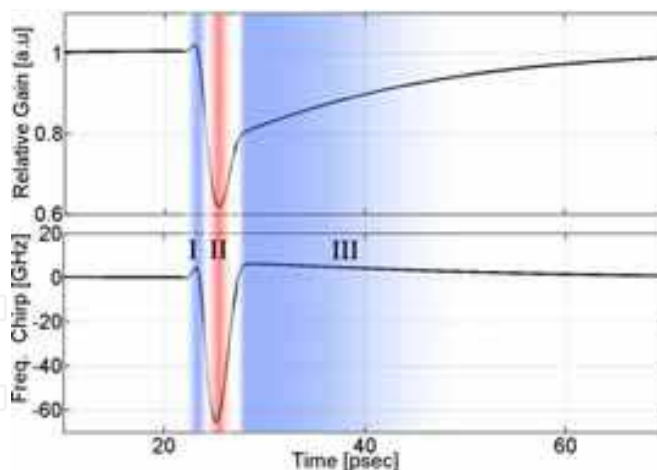Fig. 3. Operation principle of non-inverted conversion

Fig. 4. Gain and frequency shift, experienced by the probe signal

either to the left or the right of the CW probe. While filtering the red component yields a more suitable temporal pulse shape (see section II in Fig. 4, tracing the frequency chirp vs time), the sharp drop in gain implies poorer signal to noise for this option. Alternatively, opting for blue component filtering, a broader pulse is obtained but with improved signal to noise. In the experimental section below demonstration of these two filtering scheme is detailed.

Non-inverted wavelength conversion – simulation and demonstration (Raz et al, 2009)

SOA theory and numerical simulations

The final shape of the time domain pulse is dominated by the duration of the blue/red chirp induced frequency change and the shape of the optical filter used. In order to preserve the original pulse shape one needs the filter's optical bandwidth to be in the order of the spectral width of the original RZ pulses (~5 nm). Another crucial aspect for this kind of WC scheme is the eventual OSNR obtainable as it will determine the penalty incurred. For that purposes it is desired to filter out the CW component without affecting the 1st blue/red modulation side-band as it contains most of the converted pulse energy. In order to fulfill both of the above requirements a special flat top, broad filter with sharp roll off is required (Leuthold et al, 2004). In order to gain a better understanding of the requirements from this sort of filtering technique and its applicability for fast WC we used an SOA band model valid for time responses in the pico-second and sub-picosecond regime (Mork & Mecozzi, 1996; Nielsen et al, 2006; Mark & Mork, 1992; Mork & Mark, 1994). The SOA model includes XGM and XPM effects required to model the wavelength conversion process as well as Two-Photon Absorption (TPA) and Free-Carrier Absorption (FCA) responsible for the Carrier-Heating (CH) and Spectral-Hole Burning (SHB) effects. The equations used for generating the simulation results are detailed in (Mark & Mork, 1992; Mork & Mark, 1994), and are described shortly below:

$$\frac{\partial N}{\partial t} = \frac{I}{eV_c} - \frac{N}{\tau_s} - v_g g S + \frac{\Gamma_2}{\Gamma} v_g \beta_2 S^2 \tag{1}$$

$$\frac{\partial U_i}{\partial t} = (\sigma_i N \hbar \omega_0 - g E_i) v_g S + \frac{\Gamma_2}{\Gamma} v_g \beta_2 E_{2,i} S^2 - \frac{U_i - U_{L,i}}{\tau_{h,i}} \tag{2}$$

$$\frac{\partial S}{\partial z} + \frac{1}{v_g}\frac{\partial S}{\partial t} = (\Gamma g - \alpha_{\text{int}})S - \beta_2 S^2 \tag{3}$$

$$\frac{\partial p}{\partial z} + \frac{1}{v'_g}\frac{\partial p}{\partial t} = (\Gamma g - \alpha_{\text{int}})p - \beta_2 Sp \tag{4}$$

Where N stand for the carrier concentration, U_i the energy densities, and S and p represent the pump and probe photon density. The energy density is computed for both conduction ($i=c$) and (heavy hole) valence ($i=v$) band, respectively. $E_{2,i}$ are the carrier energies corresponding to the two-photon transition, i.e., $2\hbar\omega_0 = E_g + E_{2,c} + E_{2,v}$ with $\hbar\omega_0$ being the photon energy and E_g the band-gap energy, β_2 is the TPA coefficient averaged (with weight S^2) over the cross section of the waveguide (σ_i) and Γ_2 is the corresponding confinement factor for the quantum well region. We have $\Gamma_2/\Gamma > 1$ due to the tighter confinement of the square of the intensity profile, as well as the higher value for the TPA coefficient in the lower band-gap well region as compared to the separate confinement and cladding regions (Sheik-Bahae et al, 1991). In (Raz et al, 2009), a more detailed description of the simulation follows but the important results are given below in Fig. 5.
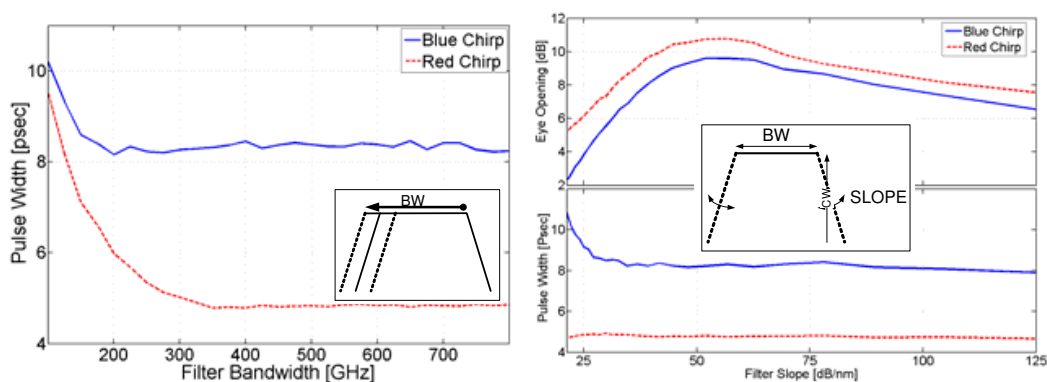

Fig. 5. Simulation results showing the dependence of pulse width on the filter Bandwidth (Left) and slope (Right)

On the left we observe the dependency of final pulse width on the bandwidth of the filter. For the case of blue chirp filtering, the slow response time sets a lower limit (8 ps) on the pulse width which is already apparent for 200 GHz filter bandwidth. However for the case of red chirp filtering the converted signal's pulse width is considerably narrower (<5 ps) and the filter bandwidth at which this value is achieved is almost double (around 400 GHz). Still it is obvious that the fundamental limit for the pulse width lies in the carrier dynamics of the SOA rather than the filter bandwidth. On the right we see how changing the filter's roll-off affects both EO and pulse width. When changing the roll-off the EO goes from a practically closed eye for a roll off lower than 25dB/nm to a maximum value of 10-11 dB for a slope value between 50-60dB/nm. Increasing the roll-off further does not improve EO as it implies sharper spectral slicing which results in ripples in the time domain eye. For EO, the difference between the red and blue filtering is not very pronounced. As for the pulse width, the same values obtained for altering the width are repeated with a minimum required roll-off larger than 30dB/nm. The apparent increase/decrease in pulse width for slopes lower than 25dB/nm is meaningless since for these values the eye is practically closes (or inverted), and only positive EO were computed as explained above.

Experimental demonstration

The experimental set-up used to demonstrate 40 and 80Gb/s direct non-inverted conversion is shown in Fig. 6
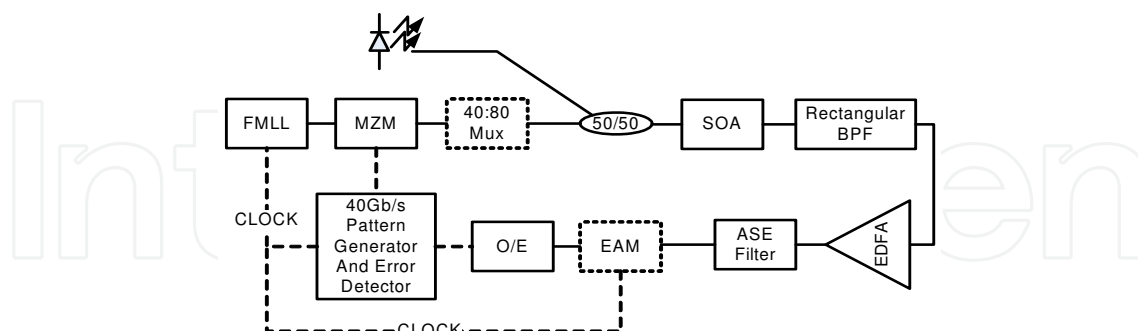

Fig. 6. Experimental set-up

40Gb/s wavelength conversion:

The 40GHz Fiber Mode Locked Laser (FMLL) RZ pulse source, with 2 ps FWHM, is externally modulated by a Mach Zehnder Modulator (MZM) by a 231-1 Pseudo Random Bit Sequence (PRBS) at 40 Gb/s. The pump signal is coupled with the probe signal and launched into the SOA. An SOA similar to the one used in (Liu et al, 2005) was also used for this experiment. The SOA has a measured total recovery time of 56 ps when biased at 400 mA, dominated by a slow blue component. At the output of the SOA the signal is filtered by the special flat top broad band filter with roll-off > 60db/nm and a rejection greater than 50dB of adjacent channels. The signal is then amplified using and Erbium doped fiber amplifiers (EDFA) and filtered again using a standard Gaussian shaped 5 nm filter to remove excess ASE noise. When running the experiment at 80Gb/s, an inter leaver is used after the modulator to go from 40 to 80 Gb/s and a EAM demux is used to gate 40Gb/s tributaries from the 80Gb/s serial data stream for BER estimation. Table 1 summarizes the key parameters for operating the WC for either the blue or red filtered components at 40Gb/s bit rate.

	Red Component Filtering	Blue Component Filtering
Pump Wavelength [nm]	1560	1560
Pump Power [dBm]	1.5	-6.3
Probe Wavelength [nm]	1548.1	1548.1
Probe Power [dBm]	1.5	-2.7
SOA current [mA]	400	262.8
Filter Center Frequency [nm]	1550.968	1545.858
Filter Bandwidth [nm]	4.5	4.31

Table 1. Main operation parameters for both blue and red filtering scenarios

In Fig. 7 the spectra for the wavelength converted signal for both filtering cases as well as the unfiltered spectrum are plotted together. The filtered spectra were taken in both cases after the EDFA so that spectral features on the edges of the filter's band-pass are lost in the ASE noise. Also, the power of the sidebands as it appears in the filtered spectra includes

~20dB of EDFA gain. The non filtered spectra, taken for the case of higher bias current and stronger pump power (green line), has a secondary peak around 1545 nm arising from non linear distortions (Self Phase Modulation) incurred by the original pump signal that are copied to the WC probe through XGM and XPM processes.
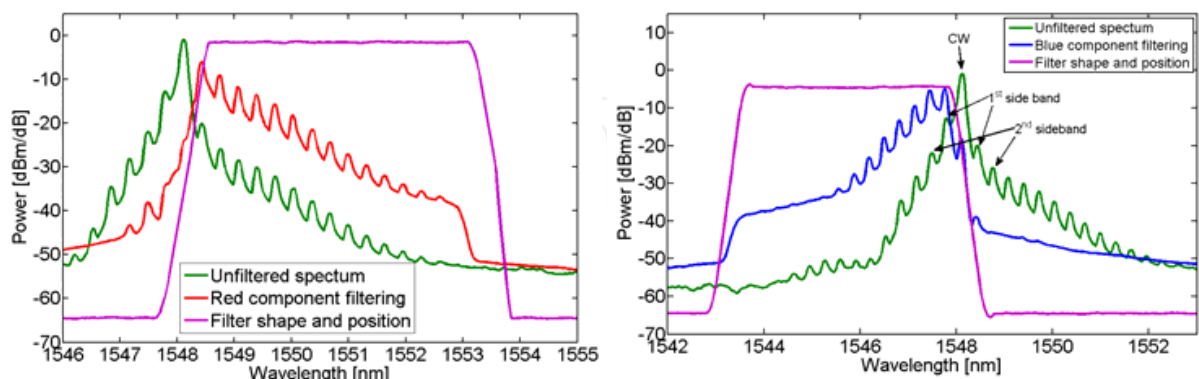

Fig. 7. Filtered and non-filtered spectra's at the SOA output

In the case of filtering out the red components, these distortions are filtered out, however for the case of blue component filtering the operating conditions had to be greatly altered (8 dB drop in pump power, and 30% drop in DC bias current for the SOA), as any distortions will be included in the broad filtered output signal.

The resulting eye patterns and Bit Error Rate (BER) vs. received power given in Fig. 8, indicate that these specific filter characteristics, especially the sharp roll-off and large band-width, greatly improve the performance of the scheme, compared with previous works. For red filtered WC there is a negligible negative penalty for BER worse than 10^{-7} but it is apparent that there is an error floor which brings the penalty for a BER of 10^{-9} to 0.5 dB. The error floor arising from the noise of the SOA is more dominant for the case of the red filtered WC since there is a power difference of 8dB between the blue and red 1st order side bands while the noise floor is the same. For the blue filtered results, a penalty of 0.7 dB is obtained and no error floor was observed.
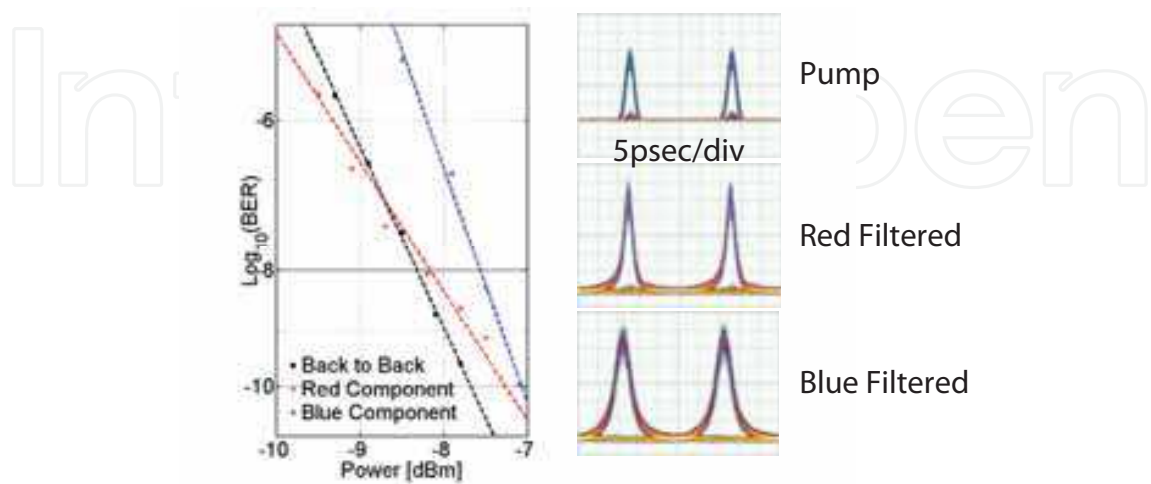

Fig. 8. BER (left) and eye patterns for B2B (top) and Red and Blue filtered (middle and bottom respectively) Wavelength converted signals

The eye patterns in Fig. 8 give an indication on the respective time domain performance for red and blue filtering. The filtering of the red components results in a much faster response with a FWHM of around 3 ps (only 1 ps more than for the original pulses, Fig. 8 top right). However for the case of filtering out the blue chirp components, which are strongly dependent on the slow recovery time of the SOA, the observed eye is much wider having a FWHM of around 4.5 ps and a pulse base duration of 12 ps.

80Gb/s wavelength conversion:

The pump signal entering the SOA is centered around 1560 nm and has a power of 0.7 dBm. The CW probe signal was at 1548.1 nm with a power of 6.7 dBm. The same SOA was used also for this experiment. At the output of the SOA a sharp flat top 6.15 nm wide Band Pass Filter (BPF) was place, centered on 1544.63 nm. The filter has a roll-off greater than 60 dB/nm and an insertion loss of 4.5 dB. After filtering, the 80 Gb/s signal is time demultiplexed to the 40 Gb/s original PRBS bit rate using Electro Absorption Modulator (EAM) gating, converted back to the electrical domain and tested for errors.

In Fig. 9, the inverted (before filter) and non-inverted spectra (taken directly after the BPF) are both shown. Notice the strong attenuation incurred by the CW signal (>35 dB) compared to the 9 dB (extra 4.5 dB due to detuning) attenuation of the 1st side band and no extra attenuation on higher order modulation side-bands. Also visible is the SOA noise floor at around -45 dBm, around the higher order side-bands. This noise together with the minimal impact on the 1st order side-band (-18 dBm) give an OSNR >25 dB, sufficiently good for the low penalty measured.
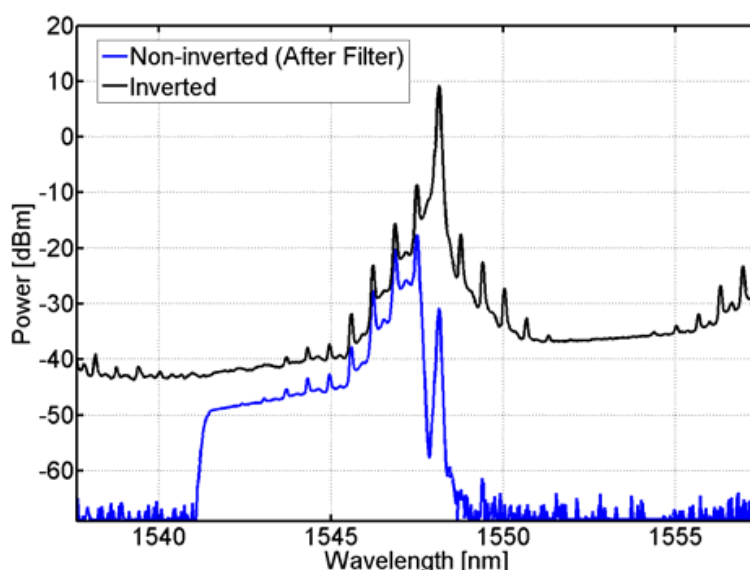

Fig. 9. Spectra of the converted signal at the output of the SOA before and after the filter

In Fig. 10 the BER for the two 40 Gb/s tributaries are shown (red lines) compared to their back to back counterparts (blue line). Also shown for comparison are the pump and probe eye patterns. The measured penalty is 0.5 dB and the eye is broadened from a 2 ps FWHM to about 4.5 ps, similar to what was measured for the experiment carried out at 40Gb/s. However the converted signal suffers from poorer OSNR leading to an observable change in BER slope.
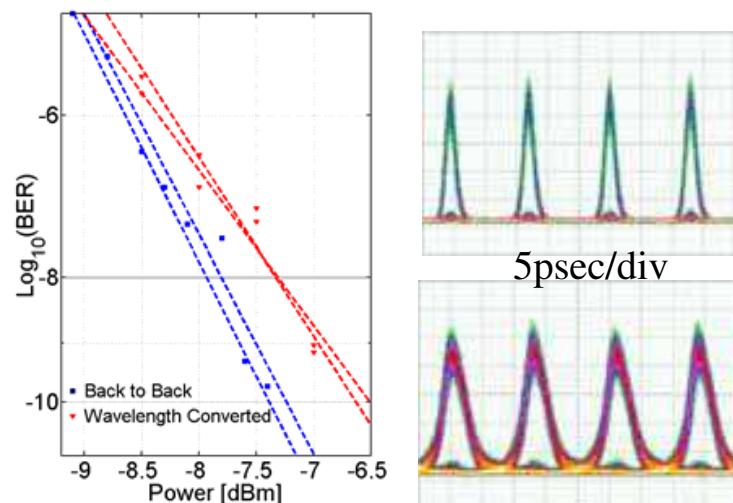
Fig. 10. BER (left) and eye patterns for B2B (blue, top right) and Wavelength converted signal (red, bottom right) respectively

3. Four Wave Mixing based wavelength convertors

The use of third order non-linearities for the purpose of all optical wavelength conversion has been demonstrated over the years in many different non-linear media. The efficiency and bandwidth of these phenomenon is governed by the third order non-linear susceptibility denoted by χ(3) and is dependent on the polarization, power, frequency detuning and dispersion of the non-linear medium used (Agrawal, 2002). In order to enhance FWM special phase matching and quasi phase matching techniques have been employed with exceptional bandwidth and efficiency demonstrated for devices based on periodically poled LiNbO3 devices (Yamawaku et al, 2003). Similarly, careful tailoring of single mode fiber dispersion, has also allowed for highly efficient FWM in highly non-linear fibers (HNLF) (Tanemura et al, 2004). However in the stride for small foot-print and low power options, a more useful solution is the employment of an SOA as a non-linear medium, as it offers integration potential and may contribute significant signal gain to offset the negative conversion efficiency.

Early studies of the nature of FWM in semiconductor traveling wave amplifiers has pointed out that the most dominant source of FWM in SOAs is the creation of gain and index gratings through the periodic modulation of the injected carriers in the device by the traveling pump and probe waves (Agrawal, 1987). Early demonstrations of wavelength conversion based on degenerate FWM in SOAs, date to the early 90', and were dedicated to the methodical characterization of the convertors in terms of conversion penalty and equivalent noise figure (Mecozzi et al, 1995; Summerfield & Tucker, 1996). In order to reduce the conversion penalty as well as lower the effective noise figure of the convertors, power levels of pump and probe signals was set so that the SOA was deeply saturated. However, high power levels, usually resulted in unwanted 2nd and 3rd order mixing products which enforced limitations on spectral spacing of pump and probe signals, especially so, for cases where multicasting conversion was demonstrated (Contestabile et al,

2004). Due to the relatively poor conversion efficiencies and high noise contribution of SOAs, the obtainable OSNR is quite limited. Thus, although FWM wavelength conversion does not suffer from time domain limitations, such as those present when performing conversion based on carrier dynamics, error free conversion for bit rates above 40Gb/s was never demonstrated. Furthermore, FWM is critically dependant on polarization alignment of pump and probe. This implies that for polarization multiplexed signals, an ever more popular bandwidth enhancement technique, FWM cannot be used in a simple manner (Contestabile et al, 2009).

In the following section recent results on FWM in SOA are detailed. These experiments focused on using a single SOA to obtain simultaneous conversion of two independent data channels. Various modulation formats and modulation speeds are explored, and a polarization insensitive set-up is also suggested.

Simultaneous FWM in SOAs (Gallep et al, 2010)

The key to the successful demonstration of simultaneous conversion of two independent data signals using FWM is proper power equalization of the input data signals as well as of the strong CW pump. Low optical power for the two input channels prevents the onset of deleterious FWM products which interfere with the converted products. However, higher input powers improve Optical Signal-to-Noise Ratio (OSNR) of the converted channels, which is essential for error-free operation. Above the optimal input power levels, used in the experiments described below, any increase in the modulated inputs does not enhance the performance but decreased the FWM efficiency due to power splitting into the non-degenerated and secondary FWM products. Similar considerations are also applied to the choice of CW-pump power: the pump must be strong enough to clamp the gain, minimizing any XGM that might be introduced by intensity modulated data inputs, and to reduce the ASE floor. On top of this optimization process, in this demonstration, it was important to obtain similar performance of the converter for single and dual operation, as it will allow for asynchronous operation. This constraint also led to a non optimal choice of probe power levels and in some cases single conversion performance could have been much better at the cost of degrading the performance of dual conversion. The choice of wavelengths (ITU channels) took into consideration the effect of unwanted conversion products between the pump and the data channels. In general the most suitable arrangement of data channels and CW pump was found to be such that the data channels are up-converted and that the spacing between them is twice as that of the spacing between the CW pump and the data channel closest to it (CW – ITU X, Data 1 – ITU X-1, Data 2 – ITU X-3). Implementation of down-conversion schemes (conversion to longer wavelengths) is not possible due inferior OSNR, 10dB lower than that achieved for up-conversion, as was pointed out already in Agrawal's seminal work of 1987 (Agrawal, 1987).

Mixed modulation formats 10 Gb/s (ASK+ PSK)

Fig. 11 presents the experimental setup used for the case of PSK and ASK simultaneous conversion at a bit rate of 10Gb/s in both channels.

The two laser sources at 1558.17 nm (-12 dBm) and 1556.55 nm (-17 dBm), ITU channels #24 and #26, were modulated with PSK and ASK respectivly at a rate of 10 Gb/s (NRZ PRBS 2^{31}-1 data sequence) and combined at the SOA input with a much stronger CW signal at 1555.75 nm (ch.#27). The polarization controllers (PC) after the lasers were carefully
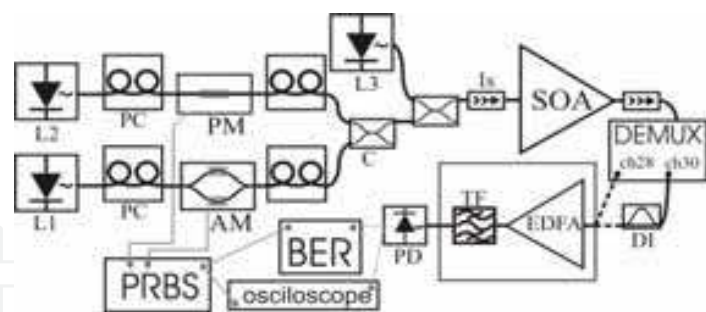
Fig. 11. Experimental setup for dual-channel (PSK + ASK) simultaneous lambda-conversion in a single SOA

adjusted to achieve the lowest insertion loss through the modulators, and the PCs just after them are used to align the polarization of the CW pump with the probe signals to maximize the FWM process. The SOA, ultra-nonlinear device with MQW structure (CIP), was biased at 500 mA, with a saturation output power of 15dBm and small signal gain >30 dB. At the output, the converted channels were filtered by an ITU-grid DEMUX (100 GHz spacing). To enable the bit-error rate (BER) versus received optical power measurements in similar conditions, the back-to-back and the converted signals were amplified by a low noise EDFA (10 dB gain, 4 dB noise figure) and filtered again (1.5 nm-window) to remove excessive ASE. The converted PSK signal was further processed by passing through a Delayed Interferometer (DI) to convert phase into amplitude modulation before detection. For the 10+10 Gb/s case the BER measurements were taken using a 10 Gb/s APD receiver.

The optical spectrum at the SOA's input and output as well as the eye diagrams and the BER vs. optical power at the receiver for the 10+10 Gb/s, ASK+PSK, are shown in Fig. 12. BER vs received optical power performance of a single converted channel is as good as the original data signal (back-to-back). Even in the presence of a 2nd converted channel the observed degradation is within the measurement error and in any case does not exceed 0.3dB.
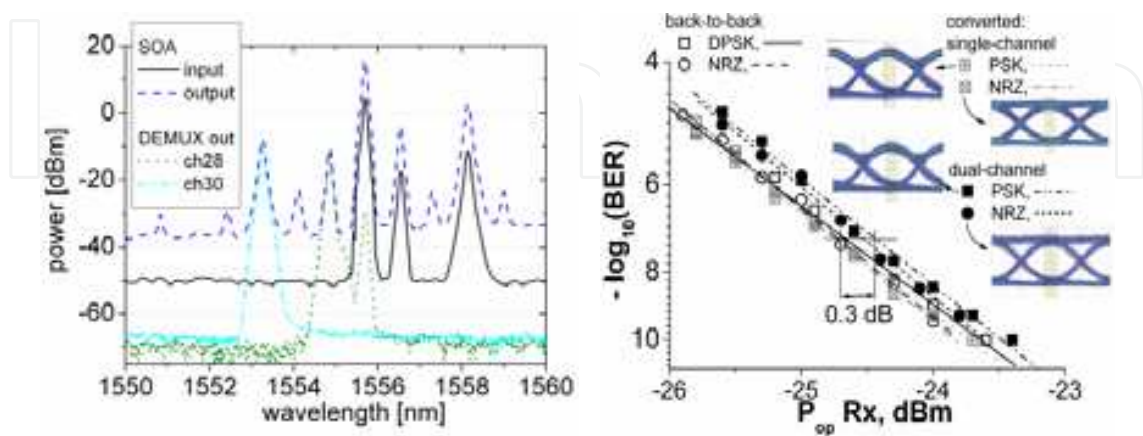

Fig. 12. Simultaneous lambda-conversion, 10+10 Gb/s (PSK+ASK): optical spectra for SOA input and output, DEMUX ch. #28 and #30 (left); eye diagrams and BER curves for single and dual conversion operation

The spectra at Fig.12 (left) illustrates the required spectral positioning of input data channels and CW pump as discussed above with the CW at ITU-grid channel #27, the ASK channel at channel #26 and the PSK channel at channel #24, avoiding interfering cross-channel products. The input PSK channel required more power (+5dB) than the ASK channel since the FWM efficiency drops the further the signal is detuned from the CW pump. In any case, this penalty-free performance is obtained for low input peak-powers (<-10 dBm) and a very modest - 2 dBm CW pump.

Mixed bit rates ASK (10+20Gb/s,10+40Gb/s)

The setup used for mixed bit rate ASK signals required several minor adaptations in comparison to the setup in Fig.11. An amplitude modulator (AM) after L2 replaced the phase modulator (PM) and a 40-Gb/s PIN photodetector replaced the APD receiver for all measured BER curves (also for the 10 Gb/s channels). In addition, the selected wavelength channels were slightly shifted in the ITU grid, but maintaining relative positioning: the CW pump at channel #28 (1554.94 nm) and the two modulated carriers at ch.#27 (1555.75 nm, L1) and ch.#25 (1557.36 nm, L2). This shift was required to better align the outputs to a 200 GHz DEMUX used to filter the converted channels out. Fig. 13 shows the measured BER vs. received power for NRZ converted channels at 10 and 20 Gb/s using a $2^{31}-1$ bits long PRBS data sequence. Optimal input power levels for data carriers were found to be below -15 dBm and the CW pump was set at +7 dBm. Both positioning of the 10 and 20 Gb/s input data channels with respect to the CW pump were tested: close to (conversion from channel #27 to ch.#29) and apart (from ch.#25 to ch.#31). From Fig. 13, the 20 Gb/s channel presents error free operation, with 1 dB degradation of required optical power at the receiver for the same BER performance when being the closest (100 GHz) to the CW probe.
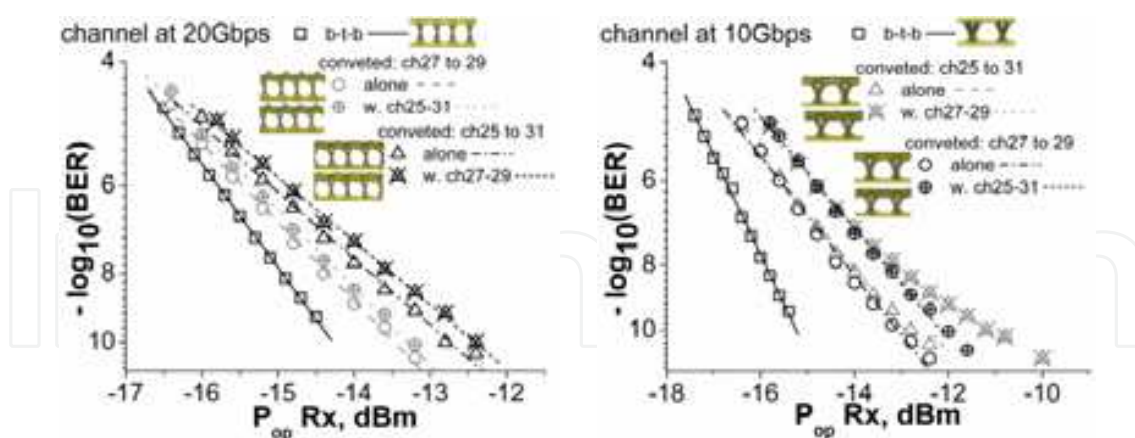

Fig. 13. Simultaneous lambda-conversion 20+10 Gb/s ASK: eye diagrams and BER curves of 20 (left) and 10 (right) Gb/s channels

When placed further away (300 GHz) the power penalty increases to 2 dB. A very small difference (0.1-0.3 dB) exists between single and dual-channel operation modes. For the 10 Gb/s channel, when placed closer to the CW pump, a power penalty of 2 dB was measured for single conversion and an extra 1.1 dB in dual-channel mode. When placed further away

from the pump (ITU ch.#25), a power penalty of 2.2 dB penalty was observed and when a 2nd channel (ch.#27) was turned on simultaneously an error floor was observed around a BER ~ 10^{-12}; at a BER of 10^{-11} a 4-dB penalty was obtained. The detected noise floor is mainly due the noise from spurious FWM over the converted channel and the limited OSNR.

For the 40+10 Gb/s case (Fig.14), the converted 40 Gb/s channel shows an error floor above BER=10^{-12} regardless of the presence of a 2nd 10 Gb/s input channel. This noise floor is mostly the result of overshoots appearing at the higher ("1") bit-level and the limited OSNR at the SOA's output.
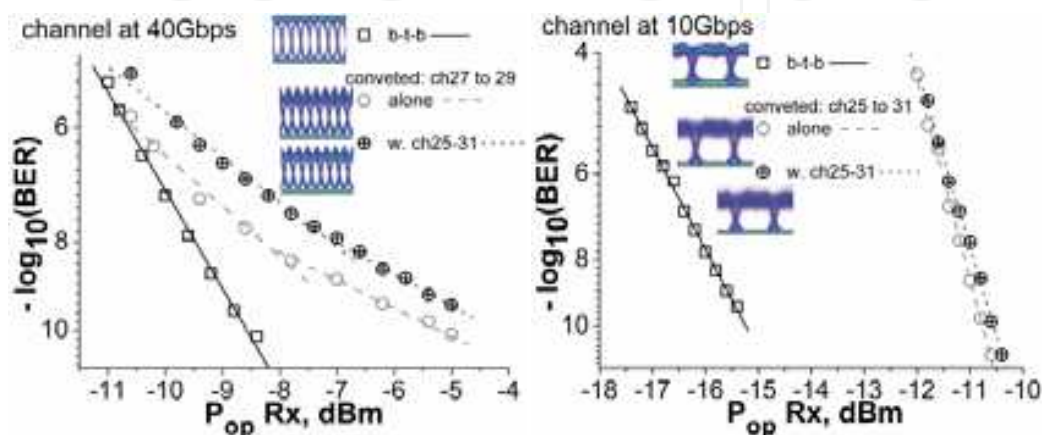

Fig. 14. Simultaneous lambda-conversion 40+10 Gb/s ASK: eye diagrams and BER curves of 40 (left) and 10 (right) Gb/s channels

A 4-dB total penalty was obtained at BER=10^{-11}, with an added 1dB penalty when the 2nd channel is turned on. The 10 Gb/s channel was measured to have a 4 dB penalty due mostly to noise over the high-level (see on inset in Fig. 14) with no difference between the single and the dual-channel operation.

For the case of simultaneous conversion of 40 and 10 Gb/s channels it was impossible to switch the respective positions of 40 and 10 Gb/s channels since the obtainable FWM efficiency and OSNR for the 40 Gb/s, when placed further away from the CW pump, could not deliver error-free operation.

Polarization insensitive simultaneous conversion (Gallep et al, 2010)

The experimental setup is presented in Fig.15(a). Each data carrier (lasers L1 and L2) passes in a polarization controller (PC) to optimize its modulator performance, with each channel modulated with PRBS 2^{31}-1 sequences and combined by a 100GHz WDM Multiplexer (MUX) with two CW probes (L3 and L4). These probes have equal power and are arranged in orthogonal polarization by passing through PCs and in a polarization beam-splitter (PBS). The combined signal is sent to the SOA, with optical isolators preventing multiple reflections. The PCs just after the modulators are used to change the relative polarization (mis)matching between the data channels and the CW carriers, and so compare the best and worst cases. The PC after the PBS is used to equalize the CW channels' gain in the SOA as well as their own degenerated FWM products' amplitudes.
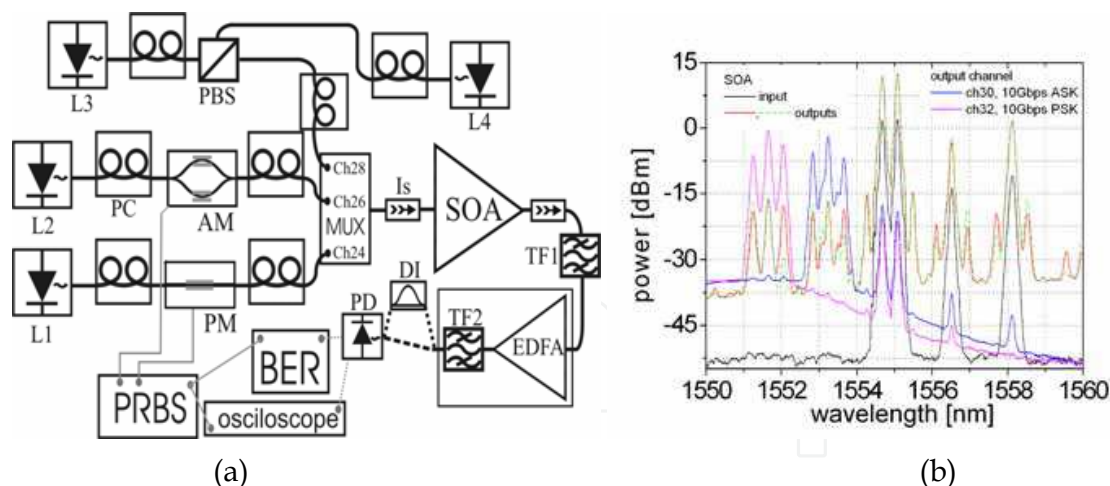
Fig. 15. Dual-channel polarization-robust AOWC: (a) the experimental setup and (b) optical spectra, for 10+10 Gb/s (ASK+PSK) operation.

For the 10+10Gb/s test the CW probes were within the ITU-grid channel number 28 (1554.94nm), and are 0.4nm apart (λL3=1554.74nm, λL4=1555.14nm); the data channels are located at channel #26 (L2, ASK) and #24 (L1, PSK). Channels #25 and #27 cannot be used since some FWM products due the interactions of the two CW probes with the input data channels are contained within their bandwidth. With this input spectra arrangement the output (converted) channels fits channels. #30 (ASK) and #32 (PSK), and are extracted by a tunable filter (TF1, 0.9nm wideband). The spectra are plotted in Fig.15(b). Once filtered the signals are further amplified by a low noise EDFA amplifier with a gain of 10dB and a noise figure of 4dB and another tunable 1.5nm wide filter (TF2) is used to remove excessive ASE before reaching the photo-diode. The detected signal is connected to a Bit-Error Rate (BER) tester to measure the performance and to an oscilloscope to obtain the eye-diagrams. The PSK channel also passes a properly tuned delay-interferometer (DI) to convert the data into ASK format.

Although the two detuned CW probes have orthogonal polarizations, some interaction between them still exists leading to FWM components on both sides of the probe signals (these signals are -30dB lower than the probes' power level). The degenerated FWM products due the interaction of each CW probe with each input channel and its replicas lead to a less then trivial spectral composition of the output channels spectra, each one with three adjacent carriers. The individual spectra contain the central (main) component, which is stable in power and two adjacent components who vary as the relative input optical polarization is changed. The small sub-peaks in the valleys in between the output ASK channels' 3 peaks (red and blue lines in Fig.15b) are due to ch.24 (PSK) FWM products, and so exclude the possibility of using the same wavelength scheme for ASK+ASK operation. The eye-diagrams and BER performance for the dual channel operation with 10+10Gb/s is shown in Fig.16, for the converted channels in the best and worst polarizations, alone or with the other carrier, as well as the back-to-back performance. The ASK output (Fig.16a) has maximum penalty of 1.5dB for the worst case, with polarization dependence between zero (single) and 0.9dB (dual channel). The PSK channel (Fig.16b) has maximum penalty of 2dB for the best case and 3dB for the worst, with minimum polarization dependence (respectively 0.3dB and 0.5dB), but presents an error-floor at 10^{-10}.
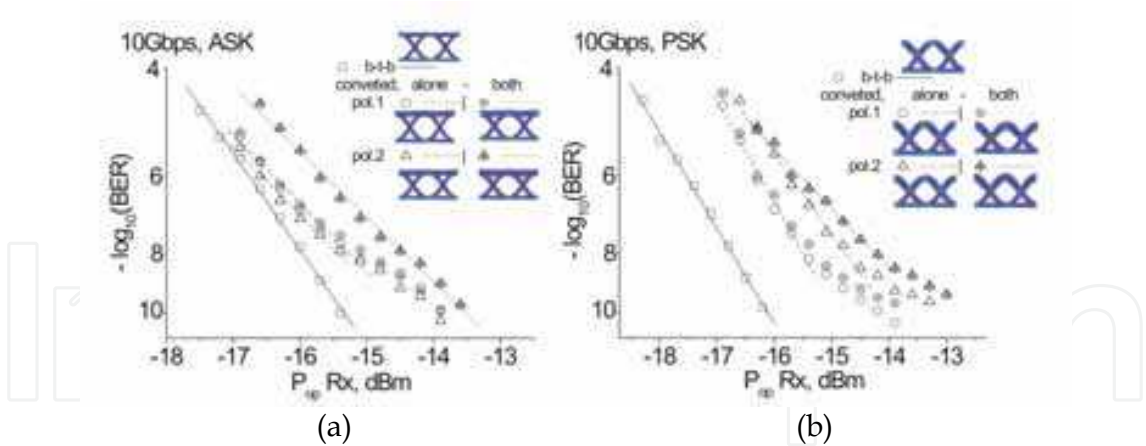
Fig. 16. BER curves and eye-diagrams (10Gbps) for dual channel conversion: (a) the ASK channel (b) the PSK channel.

This floor can be related to power fluctuation and time jitter after the PSK-to-ASK conversion in the 10GHz delayed-interferometer. With its 3 sub-carriers 50GHz apart, the output channel has reasonable part of its energy slightly detuned from the optimum point in the DI transfer function, and so some pattern dependence appears. The same setup (Fig.15a) was used to test the 20+10Gb/s, both channels in ASK. The same procedure was followed, but with the 20Gb/s input channel carrier (L2) located at ITU ch.#27, the 10Gb/s (L1) at ch.#24 and the CW probes in the ch.#29 band, and so the converted channels filtered out in the ch.#31 and ch.#34 band, with the extra channel spacing needed to avoid some 2nd order FWM that in the previous channel spacing overlapped with ch.#31's band. Fig.17 shows the eye diagrams and BER curves for the 20Gb/s (a) and 10Gb/s (b) channels and the optical spectra (c). The 20Gb/s and 10Gb/s channels have respectively maximum penalty of 2.8dB and 5.5dB for the worst polarization case, and polarization dependence respectively below 0.6dB and 0.2dB. The difference between single and dual-channel operation is larger (1.5dB) for the 10Gb/s channel in comparison with the 20Gb/s channel where it is bellow 1dB.
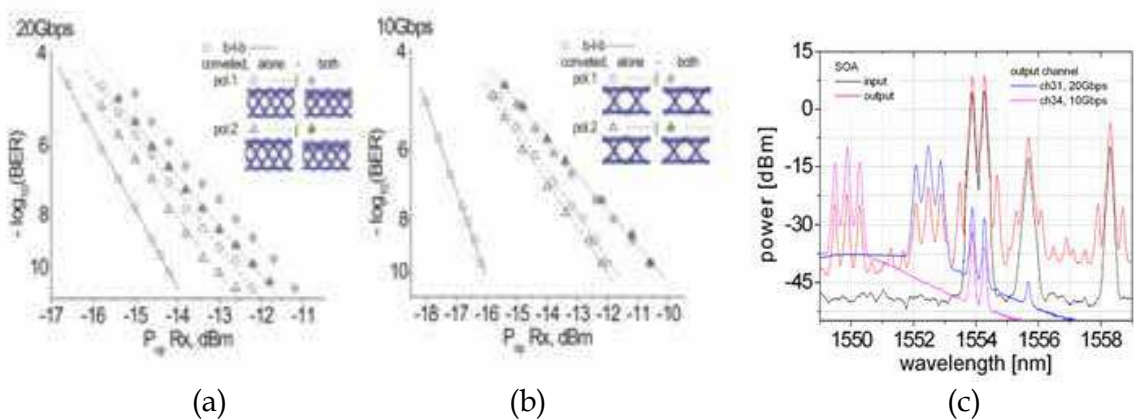

Fig. 17. BER curves and eye-diagrams for dual channel conversion (ASK+ASK): (a) the 20G channel, (b) the 10G channel; (c) optical spectra.

4. Quantom Dot SOAs

In the sections above, we have described in details how SOAs can be used for all optical wavelength conversion. One major limitation of SOAs which degrades the performance of

most of the demonstrations is the relatively high noise floor of the amplifiers. This is usually the result of the narrow gain bandwidth of the semiconductor material making the SOA, which results in substantial Amplified Spontaneous Emission (ASE) noise. Quantum dot SOAs on the other hand operate in a fundamentally different manner when compared to bulk SOAs.

The predicted superiority of quantum-dot SOAs originates from the following physical properties of quantum dots. First, gain saturation occurs primarily due to spectral hole burning even for moderate peak power smaller than 20 dBm commonly used in optical communication systems ((a) Sugawara et al, 2001; (b) Sugawara et al, 2001; (c) Sugawara et al, 2001; (d) Sugawara et al, 2001; Sugawara et al, 2002). This is due to 'slow' carrier relaxation to the ground state of about 1–100 ps (Bhattacharya, 2000; Sugawara, 1999; Marcinkevicius & Leon, 2000). The response time of gain saturation is 100 fs–1 ps ((b) Sugawara et al, 2001; Sugawara et al, 2002), which is enough for a gigabit to sub-terabit optical transmission systems. Moreover, the pattern effect is negligible, owing to the compensation of the spectral holes by the carriers relaxing from the excited states including the wetting layer, i.e. the upper states work as carrier reservoirs ((a) Sugawara et al, 2001; (b) Sugawara et al, 2001; (c) Sugawara et al, 2001; (d) Sugawara et al, 2001; Sugawara et al, 2002). Second, spatial isolation of dots prevents the transfer of carriers among dots, leading to negligible cross talk between different wavelength channels under gain saturation, when the channels are separated by more than homogeneous broadening of the single-dot gain, which is about 10–20meV at 300° K (Sakamoto & Sugawara, 2000; Sugawara et al, 2000). Third, interaction of two different wavelength channels via spatially isolated and energetically non-resonant quantum dots within the same homogeneously broadened spectral hole, causes cross gain modulation and may be used for switching functions such as wavelength conversion (Sugawara et al, 2002).

These features provide a striking contrast to bulk or quantum-well SOAs. In conventional SOAs, gain saturation occurs primarily not through spectral hole burning but rather through a reduction in the total density of carriers even for optical power levels lower than 20 dBm. This is mainly due to ultrafast intra-band carrier to carrier scattering which takes place at time constants lower than 100 fs (Kuwatsuka et al, 1999). As a result, the response time of such amplifiers to sharp changes in carrier concentration, which may be caused by a strong optical pump signal for example, is dominated by carrier recombination lifetime which is of the order of 0.1–1 ns (Agrawal & Olsson, 1989), limiting the signal processing speed. Remarkable cross talk occurs between different wavelength channels because of the continuous energy states.

Demonstration of all optical wavelength conversion using QDSOA have, similar to those carried out using bulk and quantum well devices, been carried out exploiting both conversion based on carrier dynamics (XGM and XPM) as well as those based on parametric processes (FWM). For the case of FWM, it was shown that unlike bulk or quantum well semiconductor amplifiers, where conversion efficiency to longer wavelengths is generally much lower than that in the opposite direction, this property is drastically improved, and the asymmetry between conversion directions is eliminated. This is attributed to the reduction in linewidth enhancement factor due to the discreteness of the electron states in quantum dots (Akiyama et al, 2002). Due to the scarcity of QDSOA devices, and especially for QDSOA in the popular 1.55μm communications window, much more has been written in the form of numerical and analytical studies then actual experimental results, and in the experimental field most attention was given to pump and probe experiment, focusing on

conversion efficiency and bandwidth, rather on BER performance and receiver sensitivity penalty.

For conversion based on XGM and XPM, the predicted picosecond recovery time scale has prompted a large research effort in this type of convertors. Below we detail some recently measured results of multi-casting achieved with QDSOAs at bit rates up to 40Gb/s, however recent work on this subject has also shown that using XGM and XPM good Q values for RZ eyes can be obtained up to a bit rate of 160Gb/s (Contestabile et al, 2009).

XGM+XPM based 1 to 4 Multicasting using QDSOA (Raz et al, 2008):

As explained above QDSOAs exhibit very fast recovery of gain, since ground states are filled within 0.1-1 psec. The enhanced blue chirped nature of XPM effects in QD-SOAs, when compared to bulk SOA, can be observed in Fig. 18 where the spectra's of wavelength converted inverted pulses from both a QD-SOA and a bulk SOA at 40-Gb/s RZ-PRBS are plotted. The output pulses resulting from XGM and XPM in the QD-SOAs (solid line) have a distinctly uneven spectral distribution of blue and red chirped components compared with a bulk SOA (dashed line), favoring the blue components, suggesting that the red shift is much shorter due to reduced recovery time for intra-dot processes (Akiyama et al, 2007).
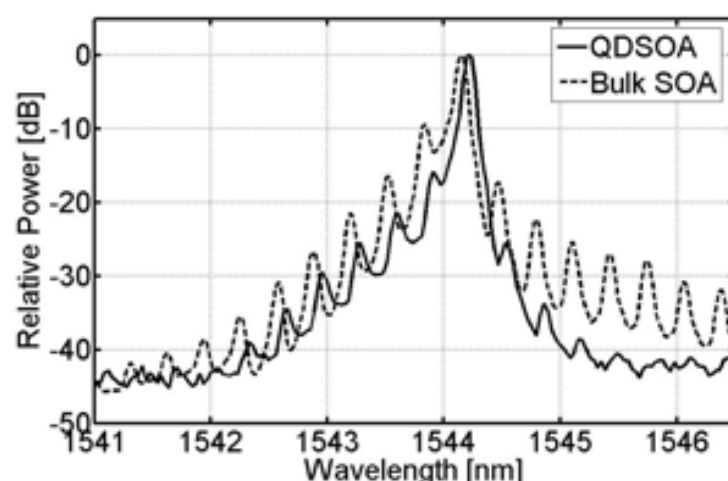

Fig. 18. The spectrum at output of a bulk SOA (dashed) compared to that of the QD-SOA (solid)

For this specific demonstration the QD-SOA we use was fabricated on an all active InP wafer. The QD material was grown on an n-type InP (100) substrate by metal–organic vapor-phase epitaxy. In the active region, five-fold stacked InAs QD layers separated by 40-nm-thick Q1.25-layer of InGaAsP were placed in the center of a 500-nm-thick lattice-matched Q1.25 waveguide core (Nötzel et al, 2006). The SOA was based on a deeply etched waveguide structure with a width of 1.6 μm, insuring single mode operation, and had a length of 2.2 mm. In order to avoid lasing, the optical waveguides were tilted by 7° and the chip-facets were anti-reflection coated. The QD-SOA was biased at 300 mA of current and cooled to 13ºC, by a thermo-electric-cooler element aided by a water cooler, the device exhibited stable and repeatable performance. Main device performance merits for the operation current of 300mA include large 3dB bandwidth (>90 nm), high saturation output power (>13 dBm) and low chip noise figure (<7 dB) as well ultra-fast 10-to-90% recovery time (<10 ps at moderate bias currents). Fiber to fiber gain was approx. -10dB due to high

coupling losses and field mismatch between the lensed fiber and the 2 micron wide deeply etched InP waveguides.

Experiment details and results:

The experimental set-up is shown in Fig. 19. The mode-locked fiber ring laser (MLFRL) emits pulses with a 1.3 ps full width at half maximum (FWHM) at 1560 nm. The channel separation for the CW probes was chosen to be 4.8 nm (≈600GHz) due to the large optical bandwidth of the short RZ pulse. The power of the modulated pump-beam in the waveguide was 7 dBm (assuming 6 dB insertion-losses at the input and output of the device) and the power for each CW signal was 3 dBm.
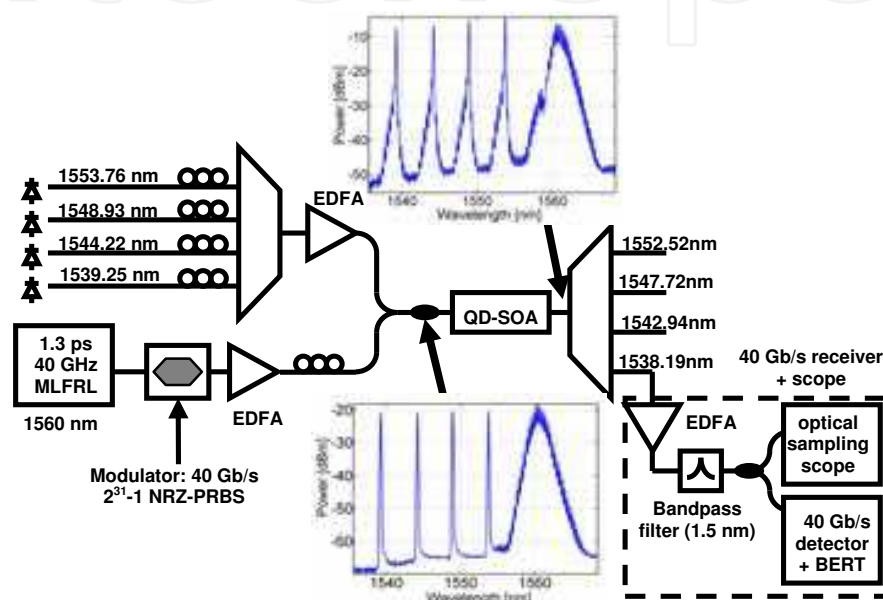

Fig. 19. Experimental set-up and optical spectra's at the QD-SOA in/output port.

Polarization controllers where used independently for each source to optimize polarization at the QD-SOA input. It is visible from the spectra of Fig. 19 that the OSNR at the QD-SOA output was larger than 42 dB. At the QD-SOA output, the channels are separated by a telecomm grade demultiplexer (DeMux). The central wavelengths of the CW signals are chosen to be +1.2 nm (≈150 GHz) detuned with respect to the central wavelengths of the DeMuX. The DeMuX had a 0.8 nm flat-top pass-band and >30 dB channel isolation. While the sharp optical filter was essential in obtaining a non-inverted output pulse, its limited pass-band resulted in a considerable pulse broadening from 1.3 to 7 ps FWHM (Fig. 20 bottom right). At the DeMuX output, the signal was further amplified and filtered to remove ASE-noise. The signals were then detected and tested for errors. BER curves for the pump signal (dashed) and the 4 converted signals (solid), as well as for a single channel under similar OSNR conditions (dash-dotted) were taken and are plotted in Fig. 20.

The measured penalty at 10-10 is in between 2 and 2.5 dB, and that for the single channel case is 2 dB. The best performing channel for the 1×4 wavelength conversion case, is that to the shortest wavelength (λ4=1539.25 nm), since it has only one adjacent signal. This channel's performance is also obtained for a 1×1 wavelength conversion (see Fig. 20 dash-dotted). The direct non-inverted error-free and low penalty, 1×4 multi-wavelength conversion, demonstrated is possible because the QD-SOA has high saturation power as
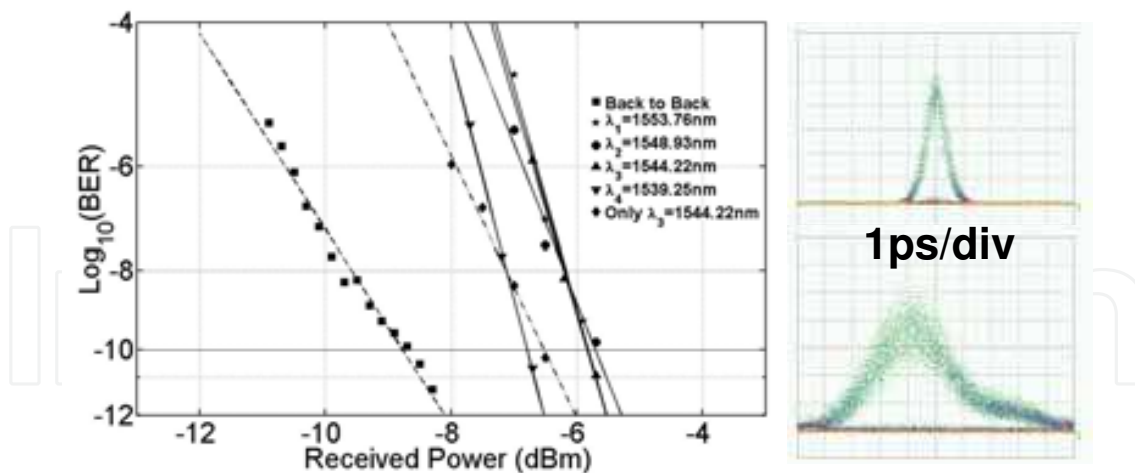
Fig. 20. Left: BER results for all the channels. Right: Eye patterns for the input and non-inverted WC output (top and bottom respectively)

well as low ASE noise. Thus when filtered out, the blue-chirp components of the output pulses have sufficient OSNR to ensure a small power penalty. The different slopes for the Back to Back and wavelength converted signals are due to the considerable broadening of the optical eye. The distorted eye is mainly due to the narrow pass bandwidth of the DeMuX and can be overcome by using a wider bandwidth filter.

5. Conclusions and future research

Semi-conductor optical amplifiers are fantastic devices for analog manipulation of light signals. Through diverse mechanisms, detailed in this chapter, it was shown that data signals at very high bit rates can be seamlessly copied from one optical carrier frequency to another. By manipulating the electrical carriers injected into the semi-conducting materials, data signals for arbitrary modulation formats have been shown to be converted through either the depletion of carriers (section 2 and 4) or the creation of index of refraction gratings (section 3). In most of the detailed demonstrations the resulting output signals are somewhat degraded, mostly due to reduced signal to noise ratio, resulting in a certain receiver sensitivity penalty. In section 4 we have also discussed how the use of novel materials, such as self assembled Quantum Dot amplifiers, can results in fast devices with improved signal to noise ratio and therefore support conversion of high speed signals.

From the overview given here it is clear that all optical wavelength conversion is a very useful application of photonic technologies. If one aims to accomplish equivalent translation of information between two optical frequencies, by moving through the electrical signal plain, the required circuit is far more complex circuit (especially so, for bit rates above 40Gb/s) and would consume far larger amounts of electrical power. Despite the obvious advantage of all optical signal processing via SOAs and the enormous research interest evident from the hundreds of scholarly publications written over the past 30 years, little if any of these methods and ideas were adopted for commercial applications. Only in the past two years there has been a slight change in the willingness to adopt such novel concepts with two high profile projects such as the MOTOR chips fabricated by UCSB (Nicholes et al, 2009) and the joint NTT & Alcatel Lucent all optical packet switch (Chiaroni et al, 2010).

In order to make SOA based all optical wavelength convertors into a main stream solution, several key developments need to take place. SOAs are essentially similar to semiconductor lasers which are being fabricated and mass manufactured for many years. The additional fiber pigtail on the second facet of the edge emitting structure, as well as the required anti-reflection coating, imply some added work and processing, but not much. Still the price of an SOA is around 2-3 orders of magnitude higher simply because the production volumes are very small. With this type of cost entry point, even the very simple SOA based wavelength convertor is more expensive then connecting, for example, two transceivers back-to-back to obtain wavelength conversion. So it is essential that prices of SOAs are sharply reduced. In addition, the noise level of SOAs remains a point of concern in case multiple hop optical networks are considered. The accumulated noise from several SOAs concatenated in an optical network, may lower the OSNR to intolerable levels. To improve signal quality, efficient optical signal re-generators need to be developed. Alternatively, further advancement of Quantum Dot amplifiers, with their low noise floor and broad gain spectrum, may prove to be extremely useful in promoting all optical wavelength conversion. On the networking side, new data transfer protocols may need to be invented which rely less on data buffering and more on exploitation of the frequency domain for the purpose of contention resolution. With these advancement there is good reason to believe that all optical wavelength conversion based on semi-conductor optical amplifiers can be am integral part of any future all optical network.

6. References

K. Inoue, "Crosstalk and its power penalty in multichannel transmission due to gain saturation in a semiconductor laser amplifier," J. Lightwave Technol., vol. 7, pp. 1118–1124, July 1989

J. Mark and J.Mork, "Sub-picosecond gain dynamics in InGaAsP optical amplifiers: Experiment and theory", Appl. Phys. Lett., 61 , 2281-2283 (1992)

CIP white paper on applications for QW SOAs, http://www.ciphotonics.com/PDFs_Jan08/SOA_Application_note_v3b.pdf

J. M. Wiesenfeld, B. Glance, J. S. Perino, A. H. Gnauck, "Wavelength Conversion at 10 Gb/s using a Semiconductor Optical Amplifier", IEEE Phot. Tech. Lett. Vol.5, No. 11,pp.1300-1303, 1993

Yasunori Miyazaki(1,2), Kazuhisa Takagi(1,2), Keisuke Matsumoto(1,2), Toshiharu Miyahara(1,2) Satoshi Nishikawa(1,2), Tatsuo Hatta(1,2), Toshitaka Aoyagi(1,2), and Kuniaki Motoshima(1,2), Polarization-Insensitive 40G-NRZ Wavelength Conversion Using SOA-MZI, Frontiers in optics 2007, FMI1]

H. Y. Yu, D. Mahgereftech, P. S. Cho, and J. Goldhar, "Optimization of the frequency response of a semiconductor optical amplifier wavelength converter using a fiber Bragg grating," J. Lightw. Technol., vol. 17, no. 2, pp. 308–315, Feb. 1999

Y. Dong, L. Lu, H. Wang, and S. Xie, "Improving performance using waveguide filter and optimal probe and signal powers for all-optical wavelength conversion," in Proc. Optical Fiber Communication (OFC), Baltimore, MD, Mar. 5–10, 2000, pp. 69–71, 2000

J. Leuthold, C. H. Joyner, B. Mikkelsen, G. Raybon, J. L. Pleumeekers, B. I. Miller, K. Dreyer, and C. A. Burrus, "100 Gb/s all-optical wavelength conversion with integrated SOA delayed-interference configuration," Electron. Lett., vol. 36, no. 13, pp. 1129–1130, Jun. 2000.

Y. Ueno, S. Nakamura, and K. Tajima, "Nonlinear phase shifts induced by semiconductor optical amplifiers with control pulses at repetition frequencies in the 40–160-GHz range for use in ultrahigh-speed all-optical signal processing," J. Opt. Soc. Amer. B, Opt. Phys., vol. 19, no. 11, pp. 2573–2589, Nov. 2002.

M. L. Nielsen and J. Mørk, "Increasing the modulation bandwidth of semiconductor-optical-amplifier-based switches by using optical filtering," J. Opt. Soc. Amer. B, Opt. Phys., vol. 21, no. 9, pp. 1606–1619, Sep. 2004.

S. Nakamura, Y. Ueno, and K. Tajima, "168-Gb/s all-optical wavelength conversion with a symmetric-Mach–Zehnder-type switch," IEEE Photon. Technol. Lett., vol. 13, no. 10, pp. 1091–1093, Oct. 2001.

Y. Liu, E. Tangdiongga, Z. Li, H. de Waardt, A. M. J. Koonen, G.D. Khoe and H.J.S. Dorren, Xuewen Shu and Ian Bennion, "Error-free 320 Gb/s SOA-based Wavelength Conversion using Optical Filtering", Proceedings of the OFC 2005, PDP28

J. Leuthold, D. M. Marom, S. Cabot, J. J. Jaques, R. Ryf, and C. R. Giles, "All-Optical Wavelength Conversion Using a Pulse Reformatting Optical Filter," Journal of Lightwave Technology, 22 , 186-192 (2004)

J. Mork and A. Mecozzi, "Theory of the ultrafast optical response of active semiconductor waveguides," Journal of Optical Society B, 13, 1803-1815 (1996)

M.L. Nielsen, J. Mørk, R. Suzuki, J. Sakaguchi, and Y. Ueno, "Experimental and theoretical investigation of the impact of ultra-fast carrier dynamics on high-speed SOA-based all-optical switches," Optics Express, 14, 331-347 (2006)

J. Mark and J.Mork, "Sub-picosecond gain dynamics in InGaAsP optical amplifiers: Experiment and theory", Appl. Phys. Lett., 61 , 2281-2283 (1992)

J. Mork and J. Mark, "Carrier heating in InGaAsP laser amplifiers due to two-photon absorption", Appl. Phys. Lett., 64 , 2206-2208 (1994)

O.Raz, J. Herrera, H.J.S. Dorren," Enhanced 40 and 80 Gb/s wavelength conversion using a rectangular shaped optical filter for both red and blue spectral slicing", Optics Express, Vol. 17, no. 3, pp. 1184-1193, 2009

Sheik-Bahae, D. C. Hutchings, D. J. Hagan, and E. W. Van Stryland, IEEE J. Quantum Electron. 27, 1296 (1991).

Y. Liu, E. Tangdiongga, Z. Li, S. Zhang, H. de Waardt, G. D. Khoe and H. J .S. Dorren, "80 Gbit/s Wavelength conversion using semiconductor optical amplifier and optical bandpass filter," Electronic Letters 41, 487-489 (2005)

Govind. P. Agrawal (2002), "*Fiber-optic Communication Systems*", John Wiley&Sons, 0-471-21571-6, USA

Jun Yamawaku et al, "Selective wavelength conversion using PPLN waveguide with two pump configuration", in conference on Lasers and Electro-optics 2003, CWB5

Takuo Tanemura et al, "Highly Efficient Arbitrary Wavelength Conversion Within Entire C-Band Based on Nondegenerate Fiber Four-Wave Mixing", IEEE Phot. Tech. Lett., Vol. 16, no. 2, pp.551-553, 2004

Govind P. Agrawal, "Four-wave mixing and phase conjugation in semiconductor laser Media", Opt. Lett., Vol.12, No.4, pp.260-262, 1987

A. Mecozzi, S. Scotti, A. D'Ottavi, E. Iannone, and P. Spano, "Four-Wave Mixing in Traveling-Wave Semiconductor Amplifiers", IEEE JQE, Vol. 31, no. 4, pp.689-699, 1995

M. A. Summerfield, R. S. Tucker, "Optimization of pump and signal powers for wavelength converters based on FWM in semiconductor optical amplifiers", IEEE Phot. Tech. Lett, Vol.8, no. 10, pp. 1316-1318, 1996

G. Contestabile, M. Presi, E. Ciaramella, "Multiple Wavelength Conversion for WDM Multicasting by FWM in an SOA", IEEE Phot. Tech. Lett, Vol. 16, no. 7, 2004

G. Contestabile et al, "Transparency of FWM in SOAs to Phase/Amplitude and Polarization", in Optical Fiber Communication Conference, paper OThM6, 2009

Cristiano M. Gallep, Harmen J.S. Dorren and Oded Raz Members IEEE," Four Wave Mixing Based Dual Wavelength Conversion in a Semiconductor Optical Amplifier", IEEE Phot. Tech. Lett, in press

C.M. Gallep, O. Raz, H.J.S. Dorren, "Polarization Independent Dual Wavelength Converter Based on FWM in a Single Semiconductor Optical Amplifier", Proceedings of the OFC 2010, OWP2, 2010

(a) M. Sugawara, N. Hatori, T. Akiyama, Y. Nakata, H. Ishikawa, Japan. J. Appl. Phys. 40 L488, 2001

(b) M. Sugawara, N. Hatori, T. Akiyama, Y. Nakata, Proc. Indium Phosphide and Related Materials '01 p 358, 2001

(c) M. Sugawara, N. Hatori, T. Akiyama, Y. Nakata, Proc. Indium Phosphide and Related Materials '01 p 471, 2001

(d) M. Sugawara, N. Hatori, T. Akiyama, Y. Nakata, H. Ishikawa, Proc. 4th Pacific Rim Conf. on Lasers and Electro-Optics p I-260, 2001

M. Sugawara, T. Akiyama, N. Hatori, Y. Nakata, Proc. Contemporary Photonics Technology 2002 p 139, 2002

A. Sakamoto, M. Sugawara, IEEE Photon. Technol.Lett. 12 pp. 107-109, 2000

M. Sugawara, K. Mukai, Y. Nakata, H. Ishikawa, Phys.Rev. B 61 pp.7595, 2000

P. Bhattacharya, IEEE JSTQE Vol. 6 pp. 426, 2000

A.V. Uskov, J. McInerney, Appl. Phys. Lett. Vol. 72 pp.58, 2000

M. Sugawara (ed) 1999 Semiconductors & Semimetals vol 60 (San Diego, CA: Academic) ch 5 p 209, 1999

S. Marcinkevicius, R. Leon, Appl. Phys. Lett. 76 2406, 2000

H. Kuwatsuka, T. Shimoyama, H. Ishikawa, IEEE JQE. Vol. 35 pp.1817, 1999

G.P. Agrawal, N.A. Olsson, IEEE JQE. Vol. 25 pp. 2297, 1989

T. Akiyama, H. Kuwatsuka, , N. Hatori, Y. Nakata, H. Ebe, M. Sugawara, "Symmetric Highly Efficient (0 dB) Wavelength Conversion Based on Four-Wave Mixing in Quantum Dot Optical Amplifiers", IEEE Phot. Tech. Lett, Vol. 14, no. 8, 2002

G. Contestabile, A. Maruta, S. Sekiguchi, K. Morito, M. Sugawara, K. Kitayama, "160 Gb/s cross gain modulation in quantum Dot SOA at 1550 nm", Proceedings of ECOC 2009, PDP. 1.4, 2009

O.Raz, J. Herrera, N. Calabretta, E. Tangdiongga, S. Anantathanasarn, R. Nötzel, H.J.S. Dorren, "Non-Inverted Multiple Wavelength Converter at 40GBs Using 1550nm Quantum Dot SOA", Electronic Letters, Vol. 44, No. 16, pp. 988-989, 2008

T. Akiyama et al, "Quantum-dot semiconductor optical amplifiers", Proceedings of the IEEE, 95, 757-1766 (2007)

R. Nötzel et al, "Self assembled InAs/InP quantum dots for telecom applications in the 1.55 μm wavelength range: Wavelength tuning, stacking, polarization control, and lasing (Review Paper)", Jpn. J. Appl. Phys., 45, 6544 (2006)

Steven C. Nicholes, Milan L. Mašanović, Biljana Jevremović, Erica Lively, Larry A. Coldren, and Daniel J. Blumenthal, "The World's First InP 8x8 Monolithic Tunable Optical Router (MOTOR) Operating at 40 Gbps Line Rate per Port", proc. of OFC 2009

Dominique Chiaroni, Géma Buforn Santamaria, Christian Simonneau, Sophie Etienne, Jean-Christophe Antona, Sébastien Bigo, Jesse Simsarian, "Packet OADMs for the next generation of ring networks ",Bell Labs Technical Journal Volume 14, Issue 4, pages 265–283, Winter 2010

Advances in Optical Amplifiers

Edited by Prof. Paul Urquhart

Optical amplifiers play a central role in all categories of fibre communications systems and networks. By compensating for the losses exerted by the transmission medium and the components through which the signals pass, they reduce the need for expensive and slow optical-electrical-optical conversion. The photonic gain media, which are normally based on glass- or semiconductor-based waveguides, can amplify many high speed wavelength division multiplexed channels simultaneously. Recent research has also concentrated on wavelength conversion, switching, demultiplexing in the time domain and other enhanced functions. Advances in Optical Amplifiers presents up to date results on amplifier performance, along with explanations of their relevance, from leading researchers in the field. Its chapters cover amplifiers based on rare earth doped fibres and waveguides, stimulated Raman scattering, nonlinear parametric processes and semiconductor media. Wavelength conversion and other enhanced signal processing functions are also considered in depth. This book is targeted at research, development and design engineers from teams in manufacturing industry, academia and telecommunications service operators.

How to reference

In order to correctly reference this scholarly work, feel free to copy and paste the following:

Oded Raz (2011). Semiconductor Optical Amplifiers and their Application for All Optical Wavelength Conversion, Advances in Optical Amplifiers, Prof. Paul Urquhart (Ed.), ISBN: 978-953-307-186-2, InTech, Available from: http://www.intechopen.com/books/advances-in-optical-amplifiers/semiconductor-optical-amplifiers-and-their-application-for-all-optical-wavelength-conversion

INTECH
open science | open minds